Thermal tunable one-dimensional photonic crystals containing phase change material*

Yuanlin Jia(贾渊琳), Peiwen Ren(任佩雯), and Chunzhen Fan(范春珍)†

School of Physics and Microstructures, Zhengzhou University, Zhengzhou 450001, *China*

(Received 10 May 2020; revised manuscript received 5 June 2020; accepted manuscript online 1 August 2020)

To obtain the adjustable photonic crystals (PCs), we numerically investigate one-dimensional (1D) PCs with alternating VO_2 and SiO_2 layers through transfer matrix method. The dispersion relation agrees well with the transmittance obtained by the finite element calculation. Tunable band gaps are achieved with the thermal stimuli of VO_2, which has two crystal structures. The monoclinic crystal structure VO_2 (R) at low temperature exhibits insulating property, and the high temperature square rutile structure VO_2 (M) presents metal state. Concretely, the bandwidth is getting narrower and red shift occurs with the higher temperature in VO_2 (R)/SiO_2 PCs structure. Based on the phase change characteristics of VO_2, we can flexibly adjust the original structure as VO_2 (R)/VO_2 (M)/SiO_2. By increasing the phase ratio of VO_2 (R) to VO_2 (M), the band gap width gradually becomes wider and blue shift occurs. The discrete layers of gradient composites on the dispersion of 1D PCs are also investigated, which enhances the feasibility in practical operation. Thus, our proposed thermal modulation PCs structure paves a new way to realize thermal tunable optical filters and sensors.

Keywords: photonic crystals, VO_2, thermal modulation, phase change

PACS: 42.70.Qs, 42.25.Bs, 81.30.Dz, 42.79.Ci **DOI:** 10.1088/1674-1056/abab78

1. Introduction

Photonic crystals (PCs) are artificial microstructures with periodic refractive index.[1] The incident electromagnetic wave scatters at the interface and the superposition of multiple scattering waves forms a photonic band gap, which is analogue to the electronic band gap in semiconductor.[2] Since the first discovery of PCs in 1987,[3,4] it can be divided into 1D,[5] 2D,[6] and 3D,[7] which has wide applications in optical fiber,[8] filter,[9] absorber,[10] and sensor.[11] The first artificial PC was fabricated in 1991, Yablonovitch drilled periodically holes in a dielectric material with a refractive index of 3.6 to achieve arbitrary angle filtering.[12] Compared with traditional PCs equipment, tunable PCs have the merits of flexible design, easy integration, and dynamic tuning. It can be achieved with the external modulation through electric,[13] magnetic,[14] optical,[15] mechanic,[16] and thermal[17] stimuli.

The emergence of liquid crystal,[18] graphene,[19] and phase change material[20] provides another way to obtain a tunable photonic band gap. In 2013, Fan *et al.* designed 1D gradient soft PCs composing of alternating ferromagnetic layers and dielectric layers to achieve magnetically regulated PCs.[21] In 2016, Liu *et al.* realized an electrically controlled optical fiber polarization filter based on liquid crystal materials.[22] In 2019, Fatemeh *et al.* used PCs with alternating layers of graphene and silica plates to achieve a tunable filter by adjusting the conductivity of graphene.[23] The phase change material VO_2 will convert from insulating phase to metal phase under thermal triggering. In 2012, Fan *et al.* designed a waveguide PC coated with VO_2 layer to implement a terahertz modulator.[24] 2D PCs containing spherical SiO_2/VO_2 core/shell nanoparticles were proposed for thermochromic smart window applications.[20] In 2017, Liang *et al.* sputtered VO_2 onto the silicon dioxide nanosphere arrays to get PCs, which have excellent near infrared modulation.[25] In 2019, Wang *et al.* developed a composite ink composed of VO_2 nanoparticles and polydimethylsiloxane to prepare 3D THz PCs by direct writing technology.[26] Even the PCs have such achievements, the challenge of active modulation still exists. Most work focused on the discrete thermal stimulation of VO_2 before or after the phase conversion. Here we theoretically investigate the influence of phase ratio between VO_2 (R) and VO_2 (M) on the dispersion relationship. Namely, the varied phase change layer with continuous thermal stimuli is fully examined.

In this paper, we have proposed 1D PCs structure with alternating VO_2 and SiO_2 layers to achieve a tunable band gap under thermal stimuli. The photonic band gap is numerical calculated with the transfer matrix method and agrees well with the finite element method (FEM). The band gap position and bandwidth of the 1D PCs are fully explored with the phase change of VO_2 from insulation phase to metal phase. Two sets of the proposed PCs structures are calculated for comparison with different portions of the phase states.

*Project supported by the Key Science and Technology Research Project of Henan Province, China (Grant No. 1721023100107).

†Corresponding author. E-mail: chunzhen@zzu.edu.cn

2. Theoretical methods

Transfer matrix method The essence of the transfer matrix method is layer by layer calculation. It is extraordinary suitable for solving the PCs system to get the dispersion relation. Now we are in the position to consider the PCs with a lattice constant d. The electromagnetic wave can be expressed as $\left[E_i(r)\ H_i(r)\right]^{\mathrm{T}}$ at the incident surface. $\left[E_i(r+d)\ H_i(r+d)\right]^{\mathrm{T}}$ can be used to represent the form of the electromagnetic wave at the exit surface. Assuming that the matrix $\boldsymbol{M}$ satisfies the relation $\left[E_i(r+d)\ H_i(r+d)\right]^{\mathrm{T}} = \boldsymbol{M}\left[E_i(r)\ H_i(r)\right]^{\mathrm{T}}$. The transmission process of electromagnetic waves in the PCs structure can be described through the transfer matrix $\boldsymbol{M}$.[27] For the 1D PCs, 2×2 transmission matrix depicts the propagation state of electromagnetic waves in each layer of the medium. The transfer matrix with TE wave can be expressed as[28]

$$\boldsymbol{M}_0^{\mathrm{TE}}(d) = \begin{bmatrix} \cos(k_1 a) & \frac{1}{k_1}\sin(k_1 a) \\ -k_1\sin(k_1 a) & \cos(k_1 a) \end{bmatrix} \begin{bmatrix} \cos(k_2 b) & \frac{1}{k_2}\sin(k_2 b) \\ -k_2\sin(k_2 b) & \cos(k_2 b) \end{bmatrix} = \begin{bmatrix} A & B \\ C & D \end{bmatrix}. \tag{1}$$

According to the Bloch theorem in the periodic system, the dispersion relationship in 1D PCs can be indicated as follows:

$$\begin{aligned} \cos(kd) &= \frac{1}{2}(A+D) \\ &= \cos(k_1 a)\cos(k_2 b) - \gamma\sin(k_1 a)\sin(k_2 b), \end{aligned} \tag{2}$$

$$\begin{aligned} \gamma &= \frac{1}{2}\left(\frac{k_2}{k_1}+\frac{k_1}{k_2}\right) \\ &= \frac{1}{2}\left(\frac{n_1\cos(\theta_1)}{n_2\cos(\theta_2)}+\frac{n_2\cos(\theta_2)}{n_1\cos(\theta_1)}\right), \end{aligned} \tag{3}$$

where $k_i = n_i\omega\cos\theta_i/c$ $(i = 1, 2)$ represents the wave vector in the medium; θ_i is the incident angle of light wave in the medium; a and b represent the thicknesses of VO_2 and SiO_2, respectively. The speed of light in vacuum is c. The dispersion relationships of the TE wave and TM wave at normal incidence $(\theta = 0^\circ)$ are the same.

Finite element method FEM is a numerical method to solve the physical field with finite boundary. The basic principle is to divide the physical field into finite elements and nodes through discretization. Then, the variables in the differential equation describing the relevant physical quantities are transformed into the interpolation function form of each element. Finally, the Maxwell's equations are discretized and solved based on the variational principle. FEM is suitable for PCs with complex structure due to its high accuracy and versatility.[29]

VO_2 has two crystal structures.[30] The monoclinic crystal structure VO_2 (R) at low temperature exhibits insulating property, and the high temperature square rutile structure VO_2 (M) presents metal state. VO_2 will convert from monoclinic crystal structure to tetragonal rutile crystal structure triggered by temperature above 68 ℃.[31] In the process of phase transition, the effective dielectric constant can be characterized with the effective medium theory[32] as follows:

$$\begin{aligned} \varepsilon_{\mathrm{eff}} &= \frac{1}{4}\{\varepsilon_{\mathrm{i}}(2-3f)+\varepsilon_{\mathrm{m}}(3f-1) \\ &\quad + \sqrt{[\varepsilon_{\mathrm{i}}(2-3f)+\varepsilon_{\mathrm{m}}(3f-1)]^2+8\varepsilon_{\mathrm{i}}\varepsilon_{\mathrm{m}}}\}, \end{aligned} \tag{4}$$

where ε_{i} is the dielectric constant of VO_2 (R) and equals to 9. The dielectric constant of VO_2 (M) can be expressed through the Drude model as $\varepsilon_{\mathrm{m}} = \varepsilon_{\mathrm{i}} + \mathrm{i}\omega_{\mathrm{p}}^2/\omega\left(\omega+\mathrm{i}\tau^{-1}\right)$, where ω_{p} is the plasma frequency and is taken as $\omega_{\mathrm{p}} = \sqrt{Ne^2/\varepsilon_0 m^*}$. The effective mass $m^* = 2m_{\mathrm{e}}$, m_{e} denotes the mass of the free electron, the carrier density $N = 8.7\times 10^{21}$ cm^{-3}, and $\tau = 2.27$ fs.[33,34] f is the volume fraction of VO_2 (M) in the entire lattice. It is a temperature dependent quantity and can be expressed as $f = 1-1/(1+\exp[(T-T_{\mathrm{C}})/\Delta T])$. The phase transition temperature is $T_{\mathrm{C}} = 341$ K, and $\Delta T = 6$ ℃ is the hysteresis temperature. The relationship between the real part of the effective dielectric constant of VO_2 and temperature in THz region is illustrated in Fig. 1. It is clearly observed that the dielectric constant gets enhanced with the increase of temperature above 341 K. It is kept as a constant in the VO_2 (R) state below 341 K and represents a dielectric layer.

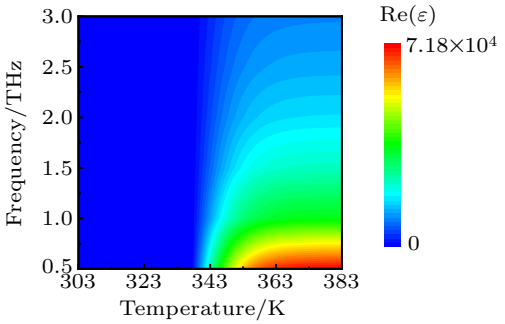

Fig. 1. Real part of the effective dielectric constant of VO_2 at different temperature in THz region.

3. Results and discussion

Figure 2 shows the 3D configuration and the cross section view of the proposed PCs structure, which is composed of alternating VO_2 (R) and SiO_2. The incident light is in TE mode along the z-axis. N denotes the period and is taken as 10. The lattice constant d is 2 μm. The thickness ratio of VO_2 (R) to SiO_2 is $a:b = 3:2$. The refractive index of SiO_2 is taken as 1.5 and the dielectric constant of VO_2 is given by Eq. (1).

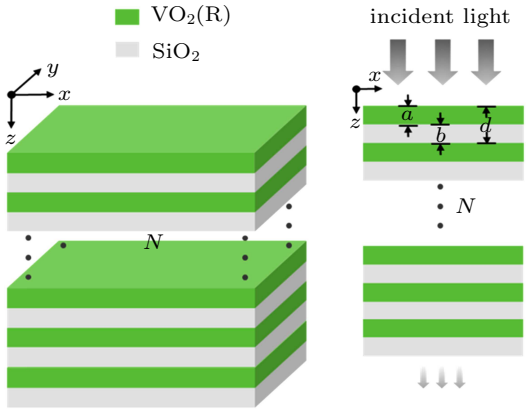

Fig. 2. The 3D configuration and the cross section view of the VO_2 (R)/SiO_2 PCs structure.

The dispersion relationship and transmittance of VO_2 (R)/SiO_2 PCs are illustrated in Fig. 3. It is obviously found that three photonic band gaps exist in the range of 0–125 THz in Fig. 3(a). The first band gap locates at 26.1–37.1 THz. The second bang gap is in the region between 56.5 THz and 73.1 THz. The third band gap is from 91.5 THz to 106.6 THz. As a result, the electromagnetic wave is not allowed to propagate through the VO_2 (R)/SiO_2 PCs in this circumstance. The corresponding transmittance of the structure is numerically shown in Fig. 3(b). It is clearly found that the transmissivity is almost zero in the photonic band gap and achieves a good self-consistent with the band gap characteristics of the PCs, verifying the correctness of our results. Besides, the transmission spectrum range is not limited to 0–125 THz. It can be extended to high frequency region with careful chosen thickness ratio. The working frequency region can be extended to 125–200 THz while the relevant parameters are taken as $d = 2$ μm and the thickness ratio of VO_2 (R) to SiO_2 is $a : b = 3 : 7$. Thus, with a smaller thickness ratio between VO_2 (R) and SiO_2, the transmission spectrum will have a significant blue shift.

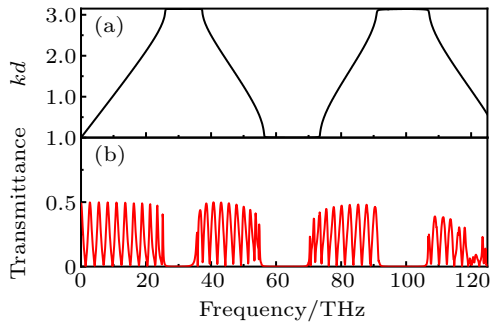

Fig. 3. (a) The dispersion relation of VO_2 (R)/SiO_2 PCs structure obtained with transfer matrix method. (b) The transmission spectrum of the structure obtained with numerical simulation.

The optical properties of VO_2 are closely related to the external temperature. Based on the phase transition characteristics of VO_2, the influences of temperature on the dispersion relationship are explored in Fig. 4. A transition from the insulating phase to the metal phase occurs at the critical temperature 341 K. In this process, there is a red shift in the dispersion relationship, and the band gap bandwidth is gradually decreasing. The first and second band gaps disappear when VO_2 is converted to metal phase at 350 K. With the phase change of VO_2 from insulating to metal phase, it is difficult for the low frequency electromagnetic waves to pass through the metallic interface due to multiple scattering overlapping. Thus, the photon band gap at low frequency will gradually disappear.

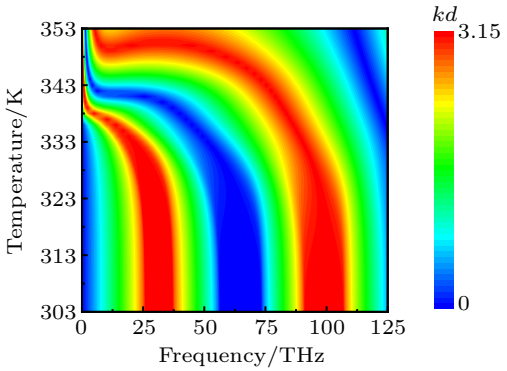

Fig. 4. The influence of temperature on the dispersion relation of VO_2 (R)/SiO_2 PCs in the range of 0–125 THz.

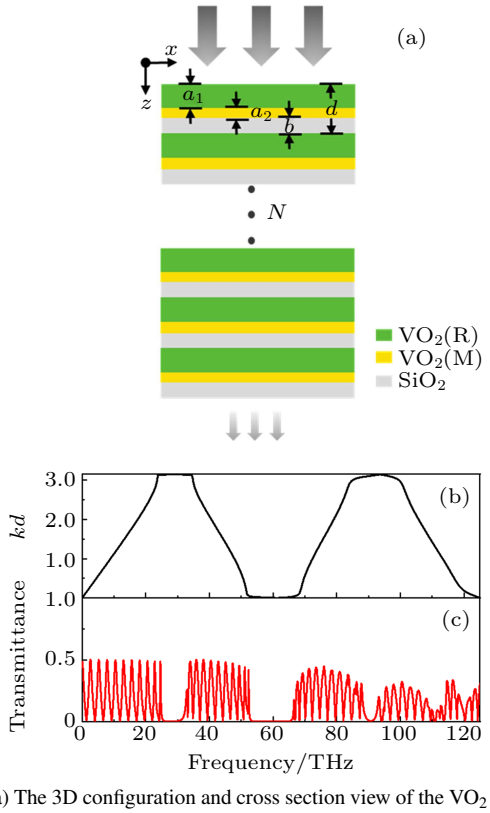

Fig. 5. (a) The 3D configuration and cross section view of the VO_2 (R)/VO_2 (M)/SiO_2 PCs structure. (b) The dispersion curve obtained with transfer matrix method. (c) The transmission spectrum of VO_2 (R)/VO_2 (M)/SiO_2 PCs structure obtained with numerical calculation.

To enrich the tunable properties of PCs, we make further adjustments to the VO_2 (R)/SiO_2 PCs structure. Now the VO_2 is divided into two parts (VO_2 (R)/VO_2 (M)). Figure 5(a) depicts 3D configuration and cross section view of the structure,

which is composed of three alternating layers VO_2 (R)/VO_2 (M)/SiO_2. a_1 and a_2 are the thicknesses of VO_2 (R) and VO_2 (M). The parameters are chosen as follows: $d = 2$ μm, $a : b = 3 : 2$, and $N = 10$. Figure 5(b) illustrates the dispersion relation and transmission spectrum with the thickness ratio $a_1 : a_2 = 5 : 1$. Compared to Fig. 3, the dispersion curve demonstrates a red shift, and the bandwidth of each band gap is getting smaller. Now the band gaps are in the ranges of 23.8–34.2 THz, 51.7–67.9 THz, and 89.5–95.8 THz respectively. In addition, the band gap will disappear in the higher frequency region. The band gap distribution in Fig. 5(b) is consistent with the transmittance in Fig. 5(c). It is revealed that the red shift of the dispersion relation and the decrease of the band gap are caused by the emergence of metal phase VO_2 (M). For the combined layer of VO_2 (R) and VO_2 (M), it can be regarded as a composite material layer. Its effective dielectric constant is obtained through series capacitance method.[35] When a new material is added to the composite layer, the effective dielectric constant of the composite layer will be reduced, resulting in the red shift of the dispersion relation and the reduction of the band gap width.

To verify the influence of VO_2 (M) on the dispersion relationship, the trend of the dispersion relationship through different thickness ratio of VO_2 (R) to VO_2 (M) is calculated in Fig. 6. The thickness ratio of $a_1 : a_2$ is from 0 to 1.0 with a thicker layer of VO_2 (R) in Fig. 6(c) and it is getting larger than 1.0 with a thicker layer of VO_2 (M) in Fig. 6(a). It can be intuitively found that the dispersion behavior of VO_2 (R) and VO_2 (M) is changing with different ratios. As the thickness of the VO_2 (M) continues to decrease, the dispersion relationship demonstrates a blue shift and the width of each band gap gradually increases. According to the series capacitance method, the effective dielectric constant of the composite layer increases with the decrease of the thickness of the metal phase. Consequently, the dielectric constant of the composite layer is significantly different from SiO_2, leading to significant band shift of PCs. Besides, the position and band gap width of the first band gap are extracted in Figs. 6(b) and 6(d). In Fig. 6(b), when the proportion of VO_2 (M) is very low, the growth trend of both is relatively flat. When the thickness of the VO_2 (M) is larger than that of the VO_2 (R), the blue shift and growth trend are obvious in Fig. 6(d). After further calculation, we extract the position distributions of the second and the third band gaps with different ratios in Fig. 7. The results denote that the variations of the second and the third band gaps are the same as that of the first band gap. Namely, as the thickness of the metal phase decreases, the dispersion relationship blue shifts and the band gaps are getting smaller.

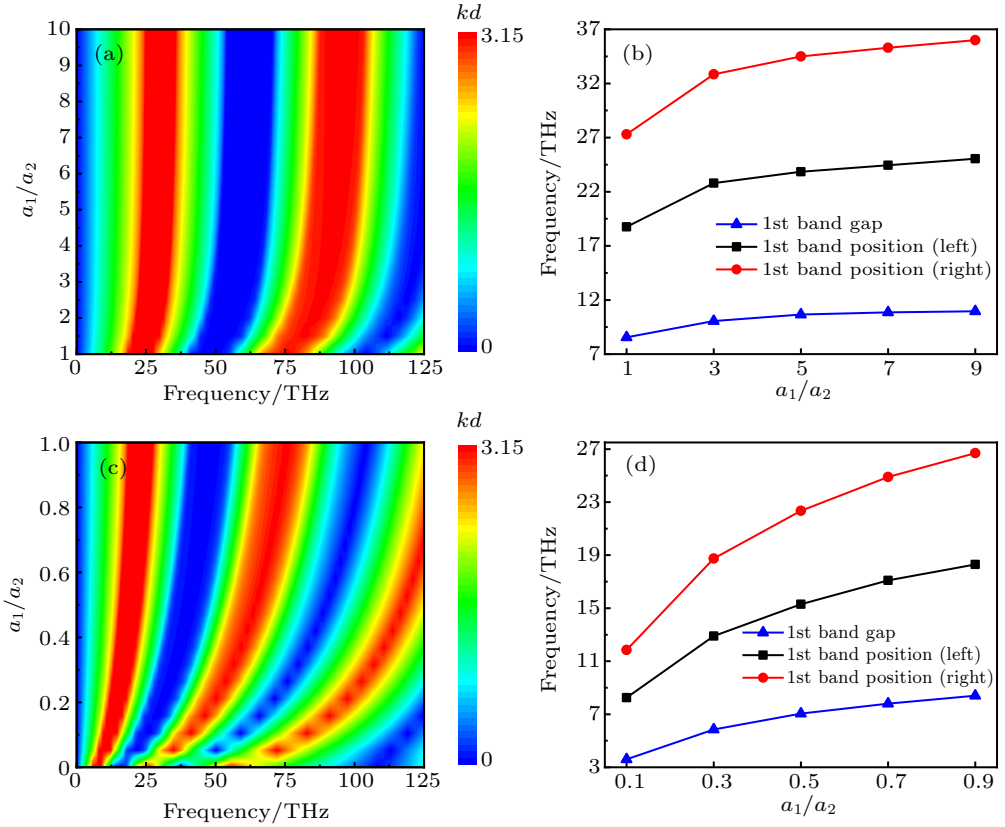

Fig. 6. (a) and (c) The influence of different proportions of VO_2 (R) and VO_2 (M), a_1/a_2, on the dispersion relation. (b) and (d) The position and band gap of the first band with different a_1/a_2.

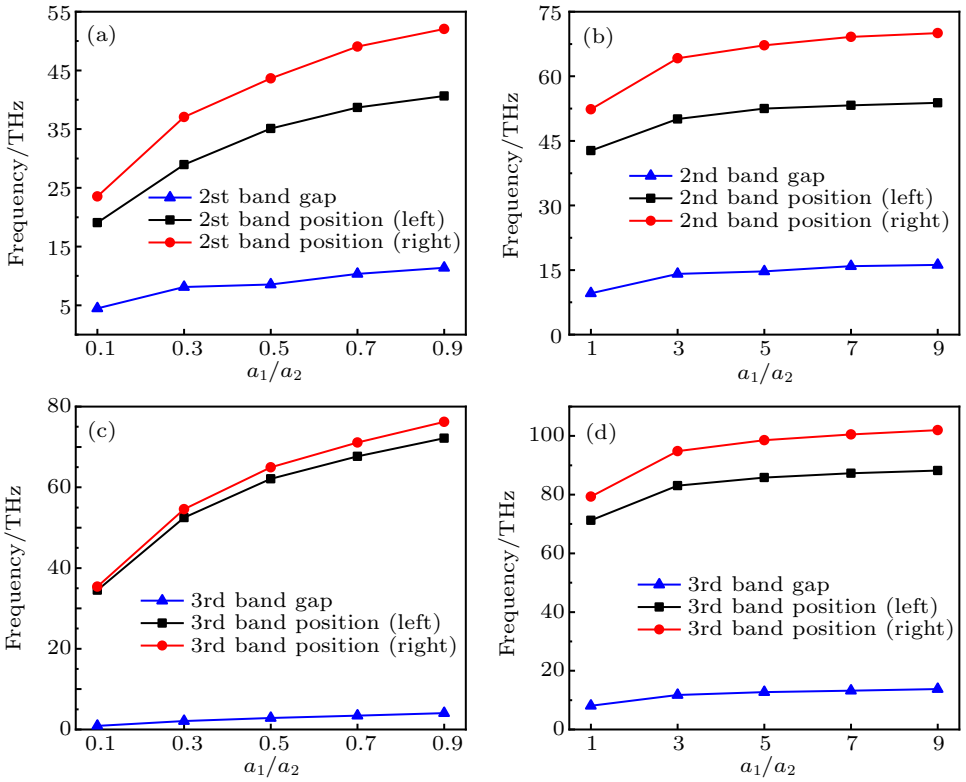

Fig. 7. (a) and (b) The position and band gap of the second band with different a_1/a_2. (c) and (d) The position and band gap of the third band with different a_1/a_2.

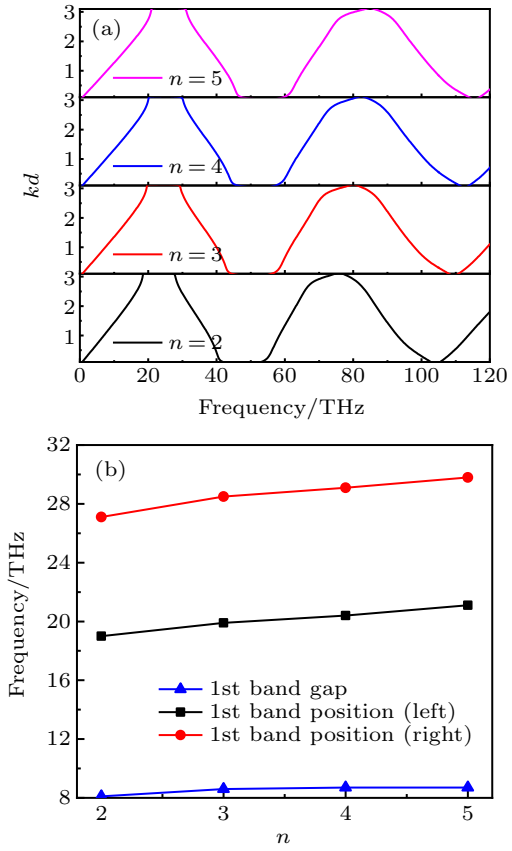

Fig. 8. (a) The dispersion curve of 1D PCs with different number of layers. (b) The position and the first band width with different layers of VO_2.

Finally, the number of layers on the dispersion of 1D PCs is considered in Fig. 8. VO_2 is divided into n layers ($n > 1$), the first and the last layers are set at 303 K (VO_2 (R)) and 343 K (VO_2 (M)). As n increases, the temperature of each layer is evenly divided. The division is listed as follows: 2 layers, $T = 303$ K, 343 K; 3 layers, $T = 303$ K, 323 K, 343 K; 4 layers, $T = 303$ K, 318 K, 333 K, 343 K; 5 layers: $T = 303$ K, 313 K, 323 K, 333 K, 343 K. Figure 8(a) presents the dispersion relationship when VO_2 is divided into different layers. When the temperature division becomes more intensive, the dispersion relationship undergoes a slight blue shift and the band gap width does not change significantly. Figure 8(b) shows the position and bandwidth of the first band gap. The band gap position is moving into higher frequency region with a larger n. The band gap width is slightly changed. Thus, to initiate the gradient temperature distribution, we can divide it into several separated parts with concrete thermal stimuli, which enhances the feasibility in practical operation.

4. Conclusion

In summary, theoretical calculation of 1D PCs consisting of alternating vanadium oxide and dielectric layer with the transfer matrix method is conducted in this work. Our results of the dispersion relation coincide well with the numerical calculation of transmittance. The position and width of the band gap can be dynamically tuned with the different phase ratios of VO_2 (R) to VO_2 (M). Thermal tunable photonic band gap can be achieved with different portions of the metallic phase of VO_2. In addition, to initiate the gradient temperature distribu-

tion, we can divide it into several separated parts with concrete thermal stimuli, which enhances the feasibility in practical operation. Therefore, this work will guide some potential applications in the thermal tunable optical filters and sensors.

References

[1] Jiang H T, Chen H, Li H Q, Zhang Y W, Zi J and Zhu S Y 2004 *Phys. Rev. E* **69** 066607
[2] Colodrero S, Ocana M and Míguez H 2008 *Langmuir* **24** 4430
[3] Yablonovitch E 1987 *Phys. Rev. Lett.* **58** 2059
[4] John S 1987 *Phys. Rev. Lett.* **58** 2486
[5] Notomi M, Kuramochi E and Taniyama H 2008 *Opt. Express* **16** 11095
[6] Fujita M, Takahashi S, Tanaka Y, Asano T and Noda S 2005 *Science* **308** 1296
[7] Noda S, Tomoda K, Yamamoto N and Chutinan A 2000 *Science* **289** 604
[8] Benabid F, Knight J C, Antonopoulos G and Russell P St J 2002 *Science* **298** 399
[9] Li S P, Liu H J, Sun Q B and Huang N 2015 *IEEE Photonic Tech. L* **27** 752
[10] Wang W Y, Cui Y X, He Y R, Lin X Y, Tian X M, Ji T and He S L 2014 *Opt. Lett.* **39** 331
[11] Zhu X, Yang X D and Wang X 2017 *Prog Electromagn Res.* **67** 103
[12] Yablonovitch E, Gmitter T J and Leung K M 1991 *Phys. Rev. Lett.* **67** 2295
[13] Jamshidi G K and Moslemi F 2017 *Appl. Opt.* **56** 4146
[14] Aly A H, Elsayed H A, Ameen A A and Mohamed S H 2017 *Int. J. Mod. Phys. B* **31** 1750239
[15] Timofeev I V, Maksimov D N and Sadreev A F 2018 *Phys. Rev. B* **97** 024306
[16] Zhao P F, Li B, Tang Z H, Gao Y, Tian H M and Chen H L 2019 *Smart Mater. Struct.* **28** 075037
[17] Zhang Y F, Chan C C and Sun J 2010 *Sens. Actuat. A-Phys.* **157** 276
[18] Busch K and John S 1999 *Phys. Rev. Lett.* **83** 967
[19] Snapp P, Kang P, Leem J and Nam S W 2019 *Adv. Funct. Mater.* **29** 1902216
[20] Ke Y J, Balin I, Wang N, Lu Q, Tok A Y, White T J, Magdassi S, Abdulhalim I and Long Y 2016 *Acs. Appl. Mater. Inter.* **8** 33112
[21] Fan C Z, Wang J Q, Zhu S M, He J N and Ding P 2013 *J. Opt.* **15** 055103
[22] Liu Q, Li S G, Li J S, Dou C, Wang X Y, Wang G Y and Shi M 2016 *J. Lightwave. Technol.* **34** 2484
[23] Ghasemi F, Entezar S R and Razi S 2019 *Phys. Lett. A* **383** 2551
[24] Fan F, Hou Y, Jiang Z W, Wang X H and Chang S J 2012 *Appl. Opt.* **51** 4589
[25] Liang J R, Li P, Song X L and Zhou L W 2017 *Appl. Phys. A* **123** 794
[26] Wang R, Yang W Y, Gao S, Ju X J, Zhu P F, Li B and Li Q 2019 *J. Mater. Chem. C* **7** 8185
[27] Suzuki M 1985 *Phys. Rev. B* **31** 2957
[28] Lin M, Ouyang Z B, Xu J and Qiu G X 2009 *Opt. Express* **17** 5861
[29] Bréchet F, Marcou J, Pagnoux D and Roy P 2000 *Opt. Fiber. Technol.* **6** 181
[30] Xiao X D, Cheng H L, Dong G P, Liu Y G, Chen L H, Miao L and Xu G 2013 *CrystEngComm* **15** 1095
[31] Kim H T, Chae B G, Youn D H, Maeng S L, Kim G, Kang K Y and Lim Y S 2004 *New J. Phys.* **6** 52
[32] Kim B J, Lee Y W, Choi S, Lim J W, Yun S J and Kim H T 2008 *Phys. Rev. B* **77** 235401
[33] Jepsen P U, Fischer B M, Thoman A and Helm H 2006 *Phys. Rev. B* **74** 205103
[34] Cocker T L, Titova L V, Fourmaux S, Bandulet H C, Brassard D, Kieffer J C, Khakani M A E and Hegmann F A 2010 *Appl. Phys. Lett.* **97** 221905
[35] Fan C Z, Wang J Q, He J N, Ding P and Liang E J 2013 *Chin. Phys. B* **22** 074211